HHS Public Access

Author manuscript

Neurobiol Dis. Author manuscript; available in PMC 2022 October 20.

Published in final edited form as:

Neurobiol Dis. 2022 October 15; 173: 105840. doi:10.1016/j.nbd.2022.105840.

Association of complement component 4 with neuroimmune abnormalities in the subventricular zone in schizophrenia and autism spectrum disorders

Ta-Chung M. Mou[a], **Malcolm V. Lane**[b], **Derek D.C. Ireland**[c], **Daniela Verthelyi**[c], **Leonardo H. Tonelli**[a,1,2], **Sarah M. Clark**[a,*,1]

[a]Laboratory of Behavioral Neuroimmunology, Department of Psychiatry, University of Maryland School of Medicine, Baltimore, MD, United States of America

[b]Department of Epidemiology and Public Health, University of Maryland School of Medicine, Baltimore, MD, United States of America

[c]Office of Biotechnology Products, US Food and Drug Administration, Silver Spring, MD, United States of America

Abstract

An early inflammatory insult is the most recognized risk factor associated with neurodevelopmental psychiatric disorders, even more so than genetic variants. Notably, complement component 4 (C4), a molecule involved in inflammatory responses, has been strongly associated with schizophrenia (SZ) and its role in other neurodevelopmental disorders, such as autism (ASD), is an area of active investigation. However, while C4 in SZ has been implicated in the context of synaptic pruning, little is known about its neuroinflammatory role. The subventricular zone (SVZ) is a region heavily involved in neurodevelopment and neuroimmune interactions through the lifespan; thus, it is a region wherein C4 may play a vital role in disease pathology. Using *in situ* hybridization with radioactive riboprobes and RNAscope, we identified robust astrocytic expression of C4 in the SVZ and in the septum pellucidum. C4 was also expressed in ependyma, neurons, and Ki67^{+} progenitor cells. Examination of mRNA levels showed elevated C4 in both ASD and SZ, with higher expression in SZ compared to controls. Targeted transcriptomic analysis of inflammatory pathways revealed a strong association

*Corresponding author at: 685 West Baltimore Street, MSTF 934-E, Baltimore, MD 21201, United States of America. sclark@som.umaryland.edu (S.M. Clark).

[1]Co-senior authors.

[2]Current affiliation of Leonardo H. Tonelli: National Institutes of Mental Health, Bethesda, MD, USA.

Declaration of Competing Interest

None.

CRediT authorship contribution statement

Ta-Chung M. Mou: Investigation, Data curation, Writing - original draft, Writing - review & editing. **Malcolm V. Lane:** Investigation. **Derek D.C. Ireland:** Investigation, Writing – review & editing. **Daniela Verthelyi:** Investigation, Writing – review & editing. **Leonardo H. Tonelli:** Conceptualization, Methodology, Supervision, Investigation, Writing - original draft, Writing - review & editing. **Sarah M. Clark:** Investigation, Data curation, Formal analysis, Supervision, Writing - original draft, Writing - review & editing.

Appendix A. Supplementary data

Supplementary data to this article can be found online at https://doi.org/10.1016/j.nbd.2022.105840.

of complement system genes with SZ, and to a lesser extent, ASD, as well as generalized immune dysregulation without a strong association with known infectious pathways. Analysis of differentially expressed genes (DEGs) showed that ASD DEGs were enriched in adaptive immune system functions such as Th cell differentiation, while SZ DEGs were enriched in innate immune system functions, including NF-κB and toll like receptor signaling. Moreover, the number of $Ki67^+$ cells was significantly higher in ASD compared to SZ and controls. Taken together, these results support a role for C4 into inflammatory-neuroimmune dysregulation observed in SZ and ASD pathology.

Keywords

Postmortem; Neuroimmune; Astrocytes; Microglia; *In situ* hybridization; Neurodevelopment; Ki67

1. Introduction

Early inflammatory challenges, such as maternal immune activation and childhood infections, are among the most recognized environmental factors contributing to neurodevelopmental disorders, including ASD and SZ (Conway and Brown, 2019; Comer et al., 2020a; Estes and McAllister, 2016; Jiang et al., 2018). Despite the different disease trajectories and clinical manifestations of these conditions, epidemiological studies have identified similar *in utero* and early-life immune dysregulation as significant risk factors (Meyer et al., 2011; Patterson, 2009). For example, viral infections during pregnancy (Atladottir et al., 2010; Brown et al., 2004), and persistent inflammatory states during gestation (Brown et al., 2014; Canetta et al., 2014), as well as autoimmune conditions (Eaton et al., 2006; Spann et al., 2019) are associated with both ASD and SZ. Furthermore, clinical case-control studies have also found that maternally derived and idiopathic brain specific autoantibodies are risk factors of ASD and SZ respectively (Braunschweig et al., 2008; Steiner et al., 2013).

Although similar environmental inflammatory factors have been attributed to these conditions, genetic studies indicate that a different set of genes confer susceptibility. Genomic studies have identified targets enriched in the regulation of gene expression and neuronal communications in ASD patients, with no immediately evident involvement of neuroimmune pathways (Grove et al., 2019; Satterstrom et al., 2020). In contrast, SZ genomic studies linked the immune response gene complement component 4 (C4) in the human leukocyte antigen (HLA) gene cluster with disease risk (Sekar et al., 2016). C4 exerts its functions in the complement cascade and immune activation by coordinating innate immune responses leading to inflammation, opsonization, pathogen lysis, and regulation of adaptive responses through antigen presentation and interactions with both B cells and T cells (Heeger and Kemper, 2012; Merle et al., 2015; Ricklin et al., 2010). In the brain, C4 and complement activation facilitate synapse elimination through microglia mediated engulfment during development and it has been proposed that this may contribute to pathological changes seen in neurodevelopmental disorders (Presumey et al., 2017). Indeed, studies have shown that enhanced expression of human C4A in mice leads to

increased microglial synaptic engulfment, reduced cortical synaptic density, and behavioral deficits (Comer et al., 2020b; Druart et al., 2021; Yilmaz et al., 2021), supporting the hypothesis that excess pruning due to C4 overexpression may be a mechanism underlying the pathophysiology of SZ (Sekar et al., 2016).

In parallel, postmortem studies have confirmed abnormal neuroimmune markers, including the upregulation of pro-inflammatory cytokine transcripts and increased microglial density and activation, in brain regions such as the cerebellum in ASD patients (Vargas et al., 2005) and the prefrontal cortex in both ASD and SZ patients (Fillman et al., 2013; Vargas et al., 2005). Due to the neurodevelopmental nature of ASD and SZ, others have specifically studied the SVZ as a region of interest (Kotagiri et al., 2014; North et al., 2021; Weissleder et al., 2021). Notably, the complement system was identified as the most upregulated pathway in the SVZ in SZ compared to controls (Weissleder et al., 2021). Not only is the SVZ a critical region during prenatal and early postnatal brain development, but it also continues to act as one of the few neurogenic niches in the adult human brain (Ernst et al., 2014; Wang et al., 2011; Weissleder et al., 2021), although ongoing adult neurogenesis in the SVZ remains controversial as others have reported conflicting results (Coletti et al., 2018; Dennis et al., 2016). However, no study has compared the expression of C4 and inflammatory molecules between ASD and SZ, conditions that share environmental risk factors but differ in genetic susceptibility. The purpose of the present study was to compare the expression of C4 between these conditions and to examine if this molecule was associated with similar or distinct immunological processes. Regional and cell type specific C4 expression patterns in the SVZ and adjacent regions were studied in relation to inflammatory molecules through targeted transcriptomics, real-time reverse transcription polymerase chain reaction (RT-PCR), and *in situ* hybridization histochemistry. RNAscope technology was used to confirm the cellular identity of C4 expressing cells. Finally, given the role of the SVZ as a potential site of adult neurogenesis, we also compared cell proliferation using Ki67.

2. Materials and methods

2.1. Postmortem brain samples

The study was reviewed and approved by the Institutional Review Board of the University of Maryland School of Medicine. Human brain samples were obtained from National Institute of Health (NIH) NeuroBioBank's brain and tissue repository at University of Maryland and the brain bank at Maryland Psychiatric Research Center. Tissue was available from a total of 65 individuals, corresponding to 24 healthy non-psychiatric controls, 21 ASD patients, and 20 SZ patients, all of which were used for *in situ* hybridization experiments. Detailed tissue characteristics and demographics for the full cohort are summarized in Supplemental (Suppl.) Table 1. Comorbid conditions included attention deficit and hyperactivity disorder ($n = 1$), developmental delay ($n = 2$), and seizure disorder ($n = 11$) for the ASD cohort, and diabetes for all three cohorts (ASD: n = 1, SZ: n = 1, Ctrl: $n = 2$). A subset of the samples ($n = 16$/group) was used for Nanostring and RT-PCR analyses (Table 1). These samples were selected based upon an attempt to as closely match available samples as possible, with a RNA integrity number (RIN) cutoff of 3.8. Limitations present in this

study include the unequal distribution of age, RIN, and postmortem interval (PMI) between groups. Additionally, there is a greater representation of Caucasian and male subjects. To account for potential impacts of these limitation on outcomes, Pearson's correlation analyses were conducted to determine if there was a significant correlation between C4 measures and age, sex, RIN, PMI, or race (Suppl. Fig. 1). If a significant correlation was detected, multiple linear regression analysis was conducted to determine if there was an interaction between disorder and the variable in question.

2.2. Tissue preparation and processing

Brain samples consisted of 25 × 25 × 15 mm fresh frozen tissue chunks from the following areas: subventricular zone (SVZ) containing adjacent corpus callosum (cc), caudate nucleus (Ca), and internal capsule (ic). Serial consecutive coronal sections of 20 um were cut in a Leica CM1900 cryostat, directly mounted onto pre-cleaned silanized glass slides for *in situ* hybridization. Adjacent sections containing the same regions were collected for RNA extraction. All collected tissues were stored at −80 °C until further histological processing or RNA extraction.

2.3. RNA extraction and quality control

RNA was extracted and purified using the phenol-chloroform-alcohol method with TRIzol reagent (Life Technologies, Carlsbad, CA, USA). Concentration and quality of the mRNA extract were determined with the Nanodrop spectrophotometer ND-1000 (ThermoFisher Scientific; Waltham, MA, USA) and by measuring 260/280 and 260/230 ratios. Total RNA samples were subsequently analyzed with Agilent 2100 Bioanalyzer (Agilent Technologies; Santa Clara, CA, USA), verifying the ratio and integrity of 18 s and 28 s rRNA bands and yielding the final RNA integrity number (RIN). For RT-PCR, 5 μg of total RNA from each case was digested with amplification grade DNase I (Invitrogen) to remove potential genomic contamination, after which RNA concentration and quality were re-checked the Nanodrop instrument.

2.4. In situ hybridization with radioactive riboprobes

A probe of 1236 bp recognizing the transcripts for both complement component 4A and B genes covering the bases 2047 to 3282 of NCBI reference sequence NM_007293.3 and a probe of 1200 bp corresponding to the marker of proliferation Ki-67 transcript variant 1 (NM_002417.5, bases 1910–3110) and variant 2 (NM_001145966.2, bases 611–1811) were cloned into the TA Dual Promoter pCR™ II vector (ThermoFisher, Cat # K205001) respectively and sequenced to confirm the length, identity, and orientation of the template sequence. Anti-sense and sense riboprobes were labeled by *in vitro* transcription in the presence of 10 μl ^{35}S-UTP (Perkin Elmer, Cat # NEG039H; Waltham, MA, USA; > 1000 Ci/mmol), 1 μg of linearized plasmid, and 20 units of T3 or T7 RNA polymerase using the MAXIscript kit (ThermoFisher, Cat # AM1324) according to the manufacturer's protocol. The *in situ* hybridization was conducted with the previously described protocol (Gunsolly et al., 2010; Tonelli et al., 2004). Hybridized sections were exposed to BioMax MR film along with ^{14}C standards (Amersham Biosciences, Cat # RPA504; Amersham, UK) for a short, medium, and long exposure time and developed in the mini medical 90 automatic film developer (AFP Imaging). All sections were assayed together in a single experiment

under the same conditions; see Suppl. Fig. 2 for representative labeling of C4 from control, ASD, and SZ sections for each exposure period. Anatomical localization of the *in situ* hybridization signals was determined by Nissl staining of adjacent sections. To resolve mRNA expression at the cellular level, a subset of slides (C4: control = 19, ASD = 19, and SZ = 12; Ki67: control = 10, ASD = 11, and SZ = 14) were coated with NTB photo emulsion (Carestream Cat # 8895666; Rochester, NY, USA), exposed for 2 months, and developed in D-19 developer substitute (Photographers' Formulary Inc., Cat # 01–0036; Condon, MT, USA) for 8 min at 20 °C, fixed for 5 min, and counterstained with toluidine blue. Positive hybridization signal was evaluated with a Leica DM6 microscope and imaged with the Leica LAS X imaging software.

2.5. RNAscope in situ hybridization

Specific probes against C4 (Cat # 544411), glial fibrillary acidic protein (GFAP; Cat # 311801), ionized calcium-binding adaptor molecule 1 (IBA1; Cat # 433121), Ki67 (Cat # 591771), neuronal nuclei protein (NeuN; Cat # 415591) mRNA transcripts were obtained from Advanced Cell Diagnotics, Inc. (ACDBio; Newark, CA, USA). Positive (3-Plex positive Control probe; Cat # 320861) and negative (dapB; Cat # 320871) control probes were included in each run using additional sections (See Suppl. Fig. 4). Hybridization was conducted according to manufacturer's instructions using the RNAscope Multiplex Fluorescent V2 Assay kit (Cat # 323110). Briefly, mounted sections were fixed in 4% PFA in PBS at 4 °C for 30 min, dehydrated in graded ethanol, and air dried. Slides underwent 0.1% H_2O_2 treatment for 10 min to quench endogenous peroxidase activity, protease plus digestion for 15 min for permeabilization, and hybridization with the C4 probe and the probe for either GFAP, NeuN, Iba-1, or Ki-67, in a hybridization oven for 2 h at 40 °C. Slides were then incubated with HRP-conjugated amplification reagents with intervening rinses in 1× washing buffer and visualized with fluorophores FITC, cyanine 3, cyanine 5 (Perkin-Elmer Cat # FP1168, 1170, and 1171), along with DAPI as the nuclear counterstain. Slides were then examined using a Leica DM6 fluorescent microscope. Additional cortical sections from unrelated cases were included to optimize the protocol; examples are shown in Suppl. Fig. 4.

2.6. Microscopy and image analysis

Autoradiographic *in situ* hybridization film images were acquired using a light table (Imaging Research Inc., Dual lamp Precision Illuminator Model B90) and a lens (Tamron, SP 28–105 mm LD) with a mounted digital camera (AMScope, MU1000). With ROI specific masks corresponding to ependymal and sub-ependymal layer of the SVZ, caudate, and corpus callosum, signal intensity was quantified using a densitometric method as previously described (Song et al., 2018); mean gray values for each image mask was measured in ImageJ software (NIH), and then transformed into nCi/mg adsorbed gray matter homogenate using the [^{3}H]Microscale calibration standard (Amersham Bioscience/ GE Healthcare, RPA504).

RNAscope images were acquired on a Leica DM6 microscope using the LASX imaging software (Leica), with DAPI (460 nm), GFP (535 nm), and Cyanine3 (610 nm) filters for multichannel fluorescence to produce tiled, maximum projection Z stacked images. Cells were considered positive if the fluorescent signal (*i.e.* puncta) co-localized with

DAPI labeled nuclei was greater than that of the neighboring background and consistent with signals yielded by the positive control probes. The negative control probe against the bacterial gene DapB further helped differentiate non-specific autofluorescent artifacts such as those produced by lipofuscin. Specific cell types were considered $C4^+$ if the cell type marker and C4 were co-localized in the same nucleus. All images were acquired under the same illumination intensity, contrast, and exposure.

2.7. Quantification of autoradiographic emulsions

Cells were considered to be positive if the density of silver grains per cell was at least four times higher than that observed in neighboring background cells and in sense control sections as previously described (Tonelli et al., 2003). For cell counting of C4, sections (1/case) were initially imaged at 50× magnification to identify the region of interest along the SVZ; 10 random images were then obtained at 400× magnification (401.62 μm × 250.93 μm) inclusive of the SVZ, but not the ependymal layer. From these images 3 were randomly selected for quantification. Using ImageJ cell counter, all cells within the field were counted (average 182 cells/field across all cases) and then all $C4^+$ cells as indicated by silver grain density (> 4× background) were counted. The average number of $C4^+$ cells and % $C4^+$ cells was then determined and averaged across cases within each group. The Average % $C4^+$ cells per section is reported in Suppl. Fig. 3. Counting of $Ki67^+$ cells was conducted by surveying the entire SVZ at 400× magnification; the total number of $Ki67^+$ cells was tallied and averaged across groups (n = 10–14; slides were selected based upon tissue integrity and preservation of the SVZ).

2.8. Image processing for figure presentation

Display adjustments for data visualization were conducted in the image acquisition software and applied uniformly to all of the images corresponding to a single experiment in the same imaging session. Images were then cropped for layout and combined in a single file using Adobe Photoshop. Adjustments to colour or brightness were applied equally across all images.

2.9. RT-PCR

RT-PCR was performed as previously described (Clark et al., 2016) using the Bio-Rad MyiQ instrument, SYBR Green Supermix (Bio-Rad; Hercules, CA, USA), and with a 3-step cycling program as follows: an initial hot start for 5 min at 95 °C followed by 40 cycles with a denaturation step of 15 s at 95 °C, an annealing step of 30 s at 55 °C, and an extension step of 30 s at 72 °C, using the primer sets listed in Supplemental Table 2. Non-template control wells were included for all genes. Relative expression for C4A, C4B, and Ki67 was determined using the $2^{-\Delta\Delta CT}$ method according to Livak and Schmittgen (2001) with the average of two housekeeping control genes, 18S and GAPDH, used for normalization.

2.10. Nanostring

Transcriptome analysis was conducted using the Nanostring Human Immunology V2 gene panel (Nanostring Technologies; Seattle, WA, USA; Cat # XT-CSO-HIM2–12). This panel comprises 594 human genes, including 15 internal reference genes for normalization. This

multiplexed analysis uses CodeSet chemistry to combine coded Reporter and Capture probes to bind to target genes which are then immobilized, aligned on a cartridge, and read using an nCounter system. In brief, a subgroup of samples of the full cohort was selected for analysis based upon demographic profile and RIN (cutoff for lowest value = 3.80) to best match samples (n = 16/group; Table 1). Purified total RNA (100 ng) was obtained from sections proximal to those used for *in situ* and RNAscope analysis as described above. Samples were hybridized overnight at 65 °C with reporter and capture probe sets and then read using the nCounter Max/Flex system (Nanostring Technologies). Samples were processed such that all groups were represented during each run. Data were acquired and analyzed using nSolver (v. 4.0; Nanostring Technologies); advanced analyses were conducted using nCounter Advanced Analysis (Nanostring Technologies) and ROSALIND (Rosa-lind, Inc., San Diego, CA, USA). Gene expression was normalized against internal reference genes and differential expression determined by fold difference compared to control samples. Volcano plots and heat maps were generated by ROSALIND.

2.11. Statistical analysis

Group comparisons were conducted using a one-way ANOVA followed by Tukey posthoc analysis for multiple comparisons (GraphPad Prism, 9.0; San Diego, CA, USA). Non-parametric data were analyzed using the Kruskal-Wallis test. Outliers were identified using the ROUT method (Q = 1%). Pearson's correlation and multiple linear regression analyses were conducted to examine relationships between C4 outcomes and demographic data. Data are presented as mean ± SEM; $p \leq 0.05$ was significant.

3. Results

3.1. C4 in situ hybridization using radioactive riboprobes

In situ hybridization using S^{35}-UTP labeled riboprobes against human C4 produced robust, dense, and specific signals in all areas surrounding the SVZ (Fig. 1A–K), with the greatest signal intensity in the septum pellucidum (SP) and the SVZ. Analysis of the hybridization signal at the cellular level showed that within the SVZ, C4 was highly abundant in the ependymal cell layer and the astrocytic ribbon (Fig. 1F). While C4 expression was ubiquitous in ependymal cells, only some of the cells in the astrocytic ribbon express C4. Similarly, C4 expression was robust in select cells in the ventricular zone proximal to the corpus callosum (cc) and along the cc-caudate (Ca) border (Fig. 1G–H). Within the SP, a majority of cells displayed strong expression of C4 with increasing density near surfaces of the lamina and along the midline (Fig. 1I). In the cc and Ca, C4 expression was less dense compared to the SVZ and SP (Fig. 1J, K). Punctate signals in the cc were associated with sparse, individual or small clusters of cells. Some positive cells in the cc were highly regular, showing the same directional organization as oligodendrocytes in the white matter bundle (Fig. 1J). $C4^+$ cells clusters were also found in the Ca. These were predominantly associated with vascular structures and in perivascular spaces rather than the lumen or the wall of the blood vessels (Fig. 1K).

3.2. C4 in situ hybridization using RNAscope

RNAscope analysis of C4 cell specific expression using probes against C4, GFAP (astrocytes), Iba1 (microglia/macrophages), and NeuN (neurons) produced highly specific signals in all areas examined. In the SVZ, C4 expression was consistent with results obtained from *in situ* hybridization with riboprobes, showing C4 spatially enriched in the ependyma. $C4^+$ cells co-labeled with GFAP were found in the astrocytic ribbon of the SVZ (Fig. 2A–B), as well as in the SP, cc (Fig. 2C), and Ca (Fig. 2D). In the cc and other areas, $Iba1^+$ microglia did not appear to express C4, but were in close proximity to $C4^+$ cells (Fig. 2E). In addition to its expression in astrocytes, C4 was also co-expressed in $NeuN^+$ neurons in the Ca (Fig. 2F). $C4^+$ astrocytes and neurons were also detected in sections of the cortex (Suppl. Fig. 5). Taken together, these results demonstrate that C4 expression occurs in diverse cell types, and regions, in the adult human brain, though it is likely that there is regional variability in expression.

3.3. RT-PCR and targeted transcriptomics

RT-PCR analysis revealed an increase in both C4A ($F_{(2, 43)} = 4.199$, $p = 0.032$) and C4B ($F_{(2, 44)} = 10.2$, $p = 0.0002$) mRNA expression. However, only SZ samples showed a significant increase compared to controls (Fig. 3A). Notably, ASD samples displayed a greater variability, reducing the overall power for this analysis (control *vs* ASD: power = 0.6, *vs* SZ: power = 0.8). Analysis of the autoradiographic films using densitometry found no differences between groups when examined by regions, including the SVZ, Ca, or cc (Suppl. Fig. 2), or in the density of C4 expressing cells in the SVZ (Suppl. Fig. 3). However, these samples were taken from the full cohort (Suppl. Table 1); thus, the discrepancy between C4 quantification by film/emulsion and RT-PCR may be explained by differences in variability in the films and/or RIN, which were partially corrected for through normalization against internal control genes using RT-PCR on a smaller cohort with less variability in RIN (Table 1). Collectively, these results suggest that increases in C4 may be due to higher expression per cell rather than an increase in the number or density of cells expressing C4.

The Nanostring Human Immunology V2 panel which probes 594 genes, was employed to further evaluate C4 expression and potential inflammatory processes in ASD and SZ ($n = 16$/group). Compared to controls, normalized gene expression values revealed 60 differentially expressed genes (DEGs; $p > 0.05$) in ASD (46 upregulated/14 downregulated; Fig. 3B) and 69 DEGs in SZ (46 upregulated/23 downregulated; Fig. 3C). ASD and SZ shared 24 DEGs (20 upregulated/4 downregulated), including C4A/B ($F(2,45) = 11.69$, $p < 0.0001$; ASD: 1.65 fold change; SZ: 2.58 fold change; Fig. 3D). Notably, most DEGs displayed only minor deviations in expression; setting a threshold of ≥ 1.5 or ≤ -1.5 fold change with an adjusted p value ≤ 0.05 restricted the number of significant DEGs to 2 genes in ASD (1 upregulated/1 down-regulated) and 13 in SZ (11 upregulated/2 down regulated).

Gene set analyses of all DEGs were used to identify underlying immune processes in these disorders. Indeed, we identified that DEGs in ASD and SZ converge on the Complement System, though to a lesser extent in ASD (Fig. 3E, F). Heatmaps of DEGs in the Complement System gene set illustrate that most of these genes are upregulated compared to controls for both ASD (Fig. 3G) and SZ (Fig. 3H). DEGs in the Complement System gene

set that are common to both ASD and SZ include C4A/B, C1R, C1S, C5, CFH, and CD46, while other DEGs differ (ASD: C1QB and CD8; SZ: CD59, SERPING1, and ITGAM). Finally, ASD and SZ also have DEGs implicated in autophagy and Nod-like receptor (NLR) signaling; however, changes in gene expression in ASD appear to be primarily associated with differentiation of Th cells (Fig. 3E), whereas DEGs in SZ are found in diverse gene sets, including those of the innate immune system, immunometabolism, Toll-like receptor (TLR) signaling, and NF-κB signaling, among others (Fig. 3F). Pathway analysis revealed a significant involvement of the Complement System in SZ (Regulation of Complement Cascade, p-Adj = 0.032; Classical Antibody-mediated complement activation; p-Adj. = 0.032), while DEGs in ASD were significantly associated with the Oncostatin M Signaling Pathway (p-Adj = 0.0015), Oxidative Damage (p-Adj = 0.0147), and Brain-Derived Neurotrophic signaling pathway (p-Adj = 0.0147). Taken together, these findings suggest that while both ASD and SZ show indications of dysregulated gene expression associated with immunological processes, there are significant differences relevant to each disorder. Furthermore, while a prior inflammatory insult may have occurred, as suggested by the identification of DEGs in the NLR signaling gene set (SZ and ASD), as well as TLR signaling and host-pathogen interaction gene sets (SZ only), gene expression levels and pathway analyses did not suggest an ongoing infectious process in SZ or ASD patients. Finally, consistent with prior results in the literature, dysregulation of the complement system was strongly associated with SZ and, to a lesser extent, ASD.

Given the limitations of this study, namely a significant difference in age between groups, differences in RIN and PMI, as well as unequal distribution of sexes and race, we conducted Pearson correlation analyses (see Suppl. Fig. 1) to determine if there was a significant relationship between any of these parameters and the quantitative outcomes for RT-PCR and Nanostring. Overall, there was a strong correlation between RT-PCR and Nanostring results for C4A and C4B, as well as between Age and measures of C4B by RT-PCR (R^2 = 0.198, p = 0.0025) and C4A/B by Nanostring (R^2 = 0.2319, p = 0.0008). However, multiple linear regression analysis did not detect a significant interaction between disorder and age for either C4B (p = 0.595) or C4A/B by Nanostring (p = 0.205). There was no significant correlation between outcomes and either sex, PMI or race; however, there was a negative correlation between RIN and C4A/B as measured by Nanostring (R^2 = 0.176, p = 0.003), but no significant interaction between RIN and disorder.

3.4. Analyses of Ki67 mRNA expression

Given the neurogenic nature of the SVZ, we examined the expression of Ki67, a canonical cell cycle marker, to determine if it was altered in ASD and SZ cohorts. *In situ* hybridization with radioactive riboprobes clearly identified the expression of Ki67 in the SVZ with positive cells regularly found in the ependyma and other layers of the SVZ (Fig. 4A–E). Furthermore, $Ki67^+$ cells were evident in the cc and Ca, both associated with blood vessel lumen and the parenchyma. RNAscope was performed to examine the relationship between Ki67 and C4 in the SVZ. In addition to cells that express only Ki67 or C4, sparse cells in the ependyma and the astrocytic ribbon co-expressed both transcripts (Fig. 4F–H). Finally, cell counting of emulsion autoradiography revealed a significant increase in $Ki67^+$ cells in the SVZ of ASD compared to both control and SZ ($F_{(2,32)}$ = 6.698, p = 0.0037; ctrl = 4.5 ±

0.7491; ASD = 9 ± 1.520; SZ = 3.286 ± 1.061; Fig. 4I). While the analysis of Ki67 mRNA expression by RT-PCR was not significant (Kruskal-Wallis, $p = 0.0566$; Fig. 4J), the results overall were consistent with the cell count. The low abundance of Ki67 mRNA transcripts, along with the small sample size, may account for the lack of statistical differences using this method. The sensitivity and cellular resolution of radioactive *in situ* hybridization may better represent group differences for this marker; however, whether these differences are biologically relevant cannot be determined by the present study.

4. Discussion

The present study revealed specific astrocytic C4 expression at the level of the anterior SVZ and the surrounding areas in the human brain. C4 was robustly expressed in the astrocytic ribbon of the SVZ and within astrocytes in the SP, as well as in the nearby Ca and cc. In addition to its abundant expression in astrocytes, C4 was also found in ependymal cells, neurons, and $Ki67^+$ putative progenitor cells in the SVZ, but not in microglia. Comparison of C4 mRNA levels revealed that the expression was significantly higher in the SVZ of SZ patients compared to that of controls. In parallel, we also found a higher density of $Ki67^+$ cells in the SVZ of ASD patients compared to controls, consistent with previous reports of increased cell proliferation in ASD (Courchesne et al., 2019; Kotagiri et al., 2014); interestingly, the latter paper also observed significantly increased GFAP immunoreactivity in the ventral SVZ in ASD brains, further suggesting astrocytic involvement in this region which may be responding to proximal cues including inflammation. Lastly, analysis of immune pathways did not provide support for infectious processes in either condition, but rather confirmed a strong association of C4 and the complement pathways with SZ, and to a lesser extent ASD. In sum, these results provide further evidence for C4's involvement in SZ and informs on its expression in the neurogenic and neuroimmune SVZ niche.

Astrocytic expression of C4 was first reported by Walker et al. (1998), showing both mRNA and protein in primary human astrocytic cultures by ELISA, RT-PCR, and immunohistochemistry. Our findings of astrocytic C4 expression in the human SVZ confirms this prior work, and, in conjunction with Sekar et al. (2016), which showed C4 protein localized to neuronal cell bodies and synapses (Suppl. Fig. 4), indicate that astrocytes may also play an important role in C4 production and activation of downstream effectors for synapse elimination. However, given that the SVZ is a neurogenic niche and not enriched in synapses or neuronal processes, C4 may exert additional, novel functions in this region. One defining role of the SVZ is its persistence as a neurogenic niche in the mature, postnatal brain (Ernst et al., 2014; Wang et al., 2011; Weissleder et al., 2021). Interestingly, we identified several $C4^+/Ki67^+$ progenitor cells within the SVZ, extending from the hypocellular gap abutting the ependyma to the astrocytic ribbon. C4 expression in progenitor cells hints at a potential role in key proliferative processes, including cell division, differentiation, and maturation, as well as apoptosis. Consistent with this, immunological control and regulation of neural stem cells through cytokine signaling has been extensively characterized in animal studies (reviewed in Gonzalez-Perez et al., 2012). Given its established role in synaptic pruning, C4 may function as part of a checkpoint mechanism to remove aberrantly dividing cells, as complement dependent elimination of neural progenitor cells was reported in a human *in vitro* study (Sellgren et al., 2017).

Furthermore, complement inhibition has been shown to promote endogenous neurogenesis in animal studies (Ducruet et al., 2012; Moriyama et al., 2011), possibly by reducing elimination of immature cells. In conjunction with significant upregulation of macrophage marker CD163 expression, increased macrophage density in the SVZ was shown to correlate with decreased expression of neurogenic markers in SZ (Weissleder et al., 2021). Thus, C4 may play an active role in coordinating peripheral immune cell trafficking and recruitment to the SVZ and further regulate adult neurogenesis in this niche. Ultimately, over-expression of C4 could potentially alter the outcomes for these processes with downstream effects on structural plasticity and brain function. Consistent with a recent report from Gallego et al. (2021) which examined C4 levels in CSF, we found an age associated increase in C4 independent of disease status, suggesting that C4 may also play a role in normal aging. Further investigation into the role of C4 in the SVZ, particularly the cell types involved and its role in early brain development, may yield additional insights into mechanisms underlying neurodevelopmental disorders, as well as aging.

In addition to the SVZ, $C4^+$ astrocytes were also found throughout both gray and white matter regions, including the caudate nucleus, cingulate cortex, cingulum, and corpus callosum, albeit less intense and numerous. Interestingly, in the SP, C4 expression and distribution in astrocytes is similar to that of the SVZ, with the densest signal in the ependyma, the layer immediately beneath the ependyma, and along the midline where the contralateral and ipsilateral lamina of the SP fuse together. Like the SVZ, the SP is perfectly poised to interact with peripheral immune cells and cytokines, due to its dense vascularization and juxtaposition to the lateral ventricles and choroid plexus, within which circulating immune surveillance cells are often found (Meeker et al., 2012). Remarkably, cavum septum pellucidum, the malformation of the SP in which two laminae fail to fuse during early development, has been reported to be more frequent in SZ (Kasai et al., 2004; Landin-Romero et al., 2016). The widespread expression of C4 in the SVZ and SP implies an essential role in normal brain functions and physiology of the periventricular system. In this regard, H. Wang et al. (2017) implicated C4a, a product of C4 activation, in the regulation of endothelial permeability, suggesting that C4 expression in the ependyma and astrocytes plays essential role in the maintenance of the blood-brain and blood-CSF barriers. Furthermore, the other product of C4 activation, C4b, participates in the classical complement activation pathway and generates potent downstream pro-inflammatory effectors (Ricklin et al., 2010), which may explain, at least in part, the hyperactivated and prolonged state of inflammation typically observed in SZ postmortem studies (Fillman et al., 2013; Trepanier et al., 2016; Volk et al., 2015). While we have established astrocytic and ependymal expression of C4 in the SVZ and surrounding regions, whether microglia express C4 in these areas remains inconclusive, as baseline C4 expression in these cells may be below detection levels for both *in situ* hybridization with radioactive riboprobes and RNAscope. In summary, C4 activation in the SVZ, SP, and the ependymal layers may serve a regulatory role in neuroimmune interactions by controlling permeability and local inflammatory responses.

Finally, inflammatory pathway analysis confirmed increased C4 expression, in addition to other complement system genes, in both ASD and SZ. While the complement system was implicated in both conditions, the magnitude was greater in SZ, consistent with prior

genomic findings (Gandal et al., 2018; Sekar et al., 2016) and further confirmed by RT-PCR analysis. In addition to upregulated complement system genes, gene set analyses revealed that key innate immune response pathways, including NF-κB, TLR signaling, and immunometabolism, were also differentially expressed in SZ. Consistent with this, NF-κB has been shown to be associated with SZ through brain proteomics (Velasquez et al., 2019), upregulated transcript expression (Volk et al., 2019), and other studies, (reviewed in Murphy et al., 2021), while TLR signaling was shown to be altered through postmortem expression analysis and genomics (Garcia-Bueno et al., 2016). In addition to altered expression of complement system genes and pathways, we found changes in genes associated with lymphocyte trafficking in SZ. These findings provide further support for SVZ RNAseq results in Weissleder et al. (2021), which reported that the upregulated genes in SZ were overrepresented in pathways related to inflammation, such as complement system (C1QA, C1QB, C4A, C3, C7), acute phase response signaling (IL1R1, SOCS3, SERPINA3), and agranulocyte adhesion and diapedesis (ITGA4, ITGA5, PECAM1). In contrast, Th cell differentiation was strongly implicated in gene set analyses in ASD, indicative of altered adaptive immunity and consistent with reports from Gupta et al. (1998) that described an imbalance in Th1 and Th2 populations in children with ASD. Changes in genes associated with Th cell differentiation may be responsible for neuroinflammation and microglial activation that have also been reported in ASD (Vargas et al., 2005). Taken together, these findings suggest a larger systemic role for T cells in the etiology of ASD. While gene expression analyses provided further evidence of immune dysregulation in SZ and ASD brains, there lacked a specific association with acute or ongoing immune activation networks directly induced by either infectious agents or foreign antigens. While we cannot rule out the presence of a peripheral infection, one possible interpretation is that complement system overactivation triggers downstream inflammatory processes, contributing to increased neuro- and systemic inflammation associated with these disorders. Indeed, a hypoactive complement system has been linked to systemic lupus erythematosus, an autoimmune disease (Walport, 2002), so it is possible that a hyperactive complement system may also result in immune dysregulation. Alternatively, elevated C4 levels may be due to age associated changes in immune function which induce an enhanced inflammatory milieu. The degree to which aging or early environmental inflammatory factors, such as maternal immune activation or childhood infections, contribute to the dysregulation of the complement system in these conditions remains to be investigated.

As previously noted, limitations present in this study include the unequal distribution of age, RIN, and PMI between groups. Additionally, there is a greater representation of Caucasian and male subjects. While the age disparity was anticipated given the different developmental trajectories of these conditions, it should be taken into consideration when interpreting differences in markers of inflammation. Differences in RIN and PMI may be due to the use of two separate tissue repositories with potentially differing specimen collection and cryopreservation protocols. Despite these limitations, we did not detect a significant interaction between C4 outcomes and either age or RIN, and we are confident in the RNA profiling performed with the current methods. In addition to these limitations, we acknowledge that the number of $Ki67^{+}$ cells in the SVZ may be influenced by a few confounds not accounted for, such as comorbid seizures (Kotagiri et al., 2014) and

antipsychotics which have been shown to increase cell proliferation (Halim et al., 2004). Finally, this study was limited to one region in the adult brain, thus, whether the changes in immune processes seen here are general-izable to the entire brain or specific to the SVZ cannot be determined.

In conclusion, the current study provides information on the anatomical distribution and cellular expression of C4, a key component in the complement system, in the SVZ of ASD and SZ patients supporting future investigations into its functional role in neuroinflammatory processes in these conditions. Taken together, evidence suggests that a similar set of environmental inflammatory risk factors in early life, acting on discrete susceptibility genes at different points during neuro-development, might yield the distinct neuroimmune pathologies of ASD and SZ.

Supplementary Material

Refer to Web version on PubMed Central for supplementary material.

Acknowledgements

The authors would like to acknowledge NIH NeuroBioBank's Brain and Tissue repository at the University of Maryland, Baltimore and Maryland Psychiatric Research Center for providing human tissues.

Funding

This work was supported by the National Institutes of Mental Health grant P50 MH103222 (Silvio O. Conte Center for Translational Mental Health Research).

Data availability

Data will be made available on request.

List of abbreviations

ASD	autism spectrum disorder
ar	astrocytic ribbon
Ca	caudate nucleus
cc	corpus callosum
Cg	cingulate cortex
C4	complement component 4
DEG	differentially regulated gene
e	ependyma
FDR	false discovery rate
GFAP	glial fibrillary acidic protein

h	hypocellular gap
HLA	human leukocyte antigen
IBA1	ionized calcium-binding adapter molecule 1
ic	internal capsule
lv	lateral ventricle
NIH	National Institute of Health
NLR	nod-like receptor
RT-PCR	reverse transcriptase polymerase chain reaction
SP	septum pellucidum
SVZ	subventricular zone
SZ	schizophrenia
TLR	toll-like receptor

References

Atladottir HO, Thorsen P, Ostergaard L, Schendel DE, Lemcke S, Abdallah M, Parner ET, 2010. Maternal infection requiring hospitalization during pregnancy and autism spectrum disorders. J. Autism Dev. Disord 40 (12), 1423–1430. 10.1007/s10803-010-1006-y. [PubMed: 20414802]

Braunschweig D, Ashwood P, Krakowiak P, Hertz-Picciotto I, Hansen R, Croen LA, Van de Water J, 2008. Autism: maternally derived antibodies specific for fetal brain proteins. Neurotoxicology 29 (2), 226–231. 10.1016/j.neuro.2007.10.010. [PubMed: 18078998]

Brown AS, Begg MD, Gravenstein S, Schaefer CA, Wyatt RJ, Bresnahan M, Susser ES, 2004. Serologic evidence of prenatal influenza in the etiology of schizophrenia. Arch. Gen. Psychiatry 61 (8), 774–780. 10.1001/archpsyc.61.8.774. [PubMed: 15289276]

Brown AS, Sourander A, Hinkka-Yli-Salomaki S, McKeague IW, Sundvall J, Surcel HM, 2014. Elevated maternal C-reactive protein and autism in a national birth cohort. Mol. Psychiatry 19 (2), 259–264. 10.1038/mp.2012.197. [PubMed: 23337946]

Canetta S, Sourander A, Surcel HM, Hinkka-Yli-Salomaki S, Leiviska J, Kellendonk C, Brown AS, 2014. Elevated maternal C-reactive protein and increased risk of schizophrenia in a national birth cohort. Am. J. Psychiatry 171 (9), 960–968. 10.1176/appi.ajp.2014.13121579. [PubMed: 24969261]

Clark SM, Pocivavsek A, Nicholson JD, Notarangelo FM, Langenberg P, McMahon RP, Tonelli LH, 2016. Reduced kynurenine pathway metabolism and cytokine expression in the prefrontal cortex of depressed individuals. J. Psychiatry Neurosci 41 (6), 386–394. 10.1503/jpn.150226. [PubMed: 27070351]

Coletti AM, Singh D, Kumar S, Shafin TN, Briody PJ, Babbitt BF, Conover JC, 2018. Characterization of the ventricular-subventricular stem cell niche during human brain development. Development 145 (20). 10.1242/dev.170100.

Comer AL, Carrier M, Tremblay ME, Cruz-Martin A, 2020a. The inflamed brain in schizophrenia: the convergence of genetic and environmental risk factors that lead to uncontrolled neuroinflammation. Front. Cell. Neurosci 14, 274. 10.3389/fncel.2020.00274. [PubMed: 33061891]

Comer AL, Jinadasa T, Sriram B, Phadke RA, Kretsge LN, Nguyen TPH, Cruz-Martin A, 2020b. Increased expression of schizophrenia-associated gene C4 leads to hypoconnectivity of prefrontal cortex and reduced social interaction. PLoS Biol. 18 (1), e3000604 10.1371/journal.pbio.3000604. [PubMed: 31935214]

Conway F, Brown AS, 2019. Maternal immune activation and related factors in the risk of offspring psychiatric disorders. Front. Psychiatry 10, 430. 10.3389/fpsyt.2019.00430. [PubMed: 31316403]

Courchesne E, Pramparo T, Gazestani VH, Lombardo MV, Pierce K, Lewis NE, 2019. The ASD living biology: from cell proliferation to clinical phenotype. Mol. Psychiatry 24 (1), 88–107. 10.1038/s41380-018-0056-y. [PubMed: 29934544]

Dennis CV, Suh LS, Rodriguez ML, Kril JJ, Sutherland GT, 2016. Human adult neurogenesis across the ages: An immunohistochemical study. Neuropathol. Appl. Neurobiol 42 (7), 621–638. 10.1111/nan.12337. [PubMed: 27424496]

Druart M, Nosten-Bertrand M, Poll S, Crux S, Nebeling F, Delhaye C, Le Magueresse C, 2021. Elevated expression of complement C4 in the mouse prefrontal cortex causes schizophrenia-associated phenotypes. Mol. Psychiatry 26 (7), 3489–3501. 10.1038/s41380-021-01081-6. [PubMed: 33837272]

Ducruet AF, Zacharia BE, Sosunov SA, Gigante PR, Yeh ML, Gorski JW, Connolly ES Jr., 2012. Complement inhibition promotes endogenous neurogenesis and sustained anti-inflammatory neuroprotection following reperfused stroke. PLoS One 7 (6), e38664. 10.1371/journal.pone.0038664. [PubMed: 22761695]

Eaton WW, Byrne M, Ewald H, Mors O, Chen CY, Agerbo E, Mortensen PB, 2006. Association of schizophrenia and autoimmune diseases: linkage of Danish national registers. Am. J. Psychiatry 163 (3), 521–528. 10.1176/appi.ajp.163.3.521. [PubMed: 16513876]

Ernst A, Alkass K, Bernard S, Salehpour M, Perl S, Tisdale J, Frisen J, 2014. Neurogenesis in the striatum of the adult human brain. Cell 156 (5), 1072–1083. 10.1016/j.cell.2014.01.044. [PubMed: 24561062]

Estes ML, McAllister AK, 2016. Maternal immune activation: implications for neuropsychiatric disorders. Science 353 (6301), 772–777. 10.1126/science.aag3194. [PubMed: 27540164]

Fillman SG, Cloonan N, Catts VS, Miller LC, Wong J, McCrossin T, Weickert CS, 2013. Increased inflammatory markers identified in the dorsolateral prefrontal cortex of individuals with schizophrenia. Mol. Psychiatry 18 (2), 206–214. 10.1038/mp.2012.110. [PubMed: 22869038]

Gallego JA, Blanco EA, Morell C, Lencz T, Malhorta AK, 2021. Complement component C4 levels in the cerebrospinal fluid and plasma of patients with schizophrenia. Neuropsychopharmacology 46 (6), 1140–1144. 10.1038/s41386-020-00867-6. [PubMed: 32961544]

Gandal MJ, Haney JR, Parikshak NN, Leppa V, Ramaswami G, Hartl C, Geschwind DH, 2018. Shared molecular neuropathology across major psychiatric disorders parallels polygenic overlap. Science 359 (6376), 693–697. 10.1126/science.aad6469. [PubMed: 29439242]

Garcia-Bueno B, Gasso P, MacDowell KS, Callado LF, Mas S, Bernardo M, Leza JC, 2016. Evidence of activation of the toll-like receptor-4 proinflammatory pathway in patients with schizophrenia. J. Psychiatry Neurosci 41 (3), E46–E55. 10.1503/jpn.150195. [PubMed: 27070349]

Gonzalez-Perez O, Gutierrez-Fernandez F, Lopez-Virgen V, Collas-Aguilar J, Quinones-Hinojosa A, Garcia-Verdugo JM, 2012. Immunological regulation of neurogenic niches in the adult brain. Neuroscience 226, 270–281. 10.1016/j.neuroscience.2012.08.053. [PubMed: 22986164]

Grove J, Ripke S, Als TD, Mattheisen M, Walters RK, Won H, Borglum AD, 2019. Identification of common genetic risk variants for autism spectrum disorder. Nat. Genet 51 (3), 431–444. 10.1038/s41588-019-0344-8. [PubMed: 30804558]

Gunsolly C, Nicholson JD, Listwak SJ, Ledee D, Zelenka P, Verthelyi D, Tonelli LH, 2010. Expression and regulation in the brain of the chemokine CCL27 gene locus. J. Neuroimmunol 225 (1–2), 82–90. 10.1016/j.jneuroim.2010.04.019. [PubMed: 20605223]

Gupta S, Aggarwal S, Rashanravan B, Lee T, 1998. Th1- and Th2-like cytokines in CD4+ and CD8+ T cells in autism. J. Neuroimmunol 85 (1), 106–109. 10.1016/s0165-5728(98)00021-6. [PubMed: 9627004]

Halim ND, Weickert CS, McClintock BW, Weinberger DR, Lipska BK, 2004. Effects of chronic haloperidol and clozapine treatment on neurogenesis in the adult rat hippocampus. Neuropsychopharmacology 29 (6), 1063–1069. 10.1038/sj.npp.1300422. [PubMed: 15010699]

Heeger PS, Kemper C, 2012. Novel roles of complement in T effector cell regulation. Immunobiology 217 (2), 216–224. 10.1016/j.imbio.2011.06.004. [PubMed: 21742404]

Jiang NM, Cowan M, Moonah SN, Petri WA Jr., 2018. The impact of systemic inflammation on neurodevelopment. Trends Mol. Med 24 (9), 794–804. 10.1016/j.molmed.2018.06.008. [PubMed: 30006148]

Kasai K, McCarley RW, Salisbury DF, Onitsuka T, Demeo S, Yurgelun-Todd D, Shenton ME, 2004. Cavum septi pellucidi in first-episode schizophrenia and first-episode affective psychosis: an MRI study. Schizophr. Res 71 (1), 65–76. 10.1016/j.schres.2003.12.010. [PubMed: 15374574]

Kotagiri P, Chance SA, Szele FG, Esiri MM, 2014. Subventricular zone cytoarchitecture changes in autism. Dev. Neurobiol 74 (1), 25–41. 10.1002/dneu.22127. [PubMed: 24002902]

Landin-Romero R, Amann BL, Sarro S, Guerrero-Pedraza A, Vicens V, Rodriguez-Cano E, Radua J, 2016. Midline brain abnormalities across psychotic and mood disorders. Schizophr. Bull 42 (1), 229–238. 10.1093/schbul/sbv097. [PubMed: 26187283]

Livak KJ, Schmittgen TD, 2001. Analysis of relative gene expression data using real-time quantitative PCR and the 2(-Delta Delta C(T)) method. Methods 25 (4), 402–408. 10.1006/meth.2001.1262. [PubMed: 11846609]

Meeker RB, Williams K, Killebrew DA, Hudson LC, 2012. Cell trafficking through the choroid plexus. Cell Adhes. Migr 6 (5), 390–396. 10.4161/cam.21054.

Merle NS, Noe R, Halbwachs-Mecarelli L, Fremeaux-Bacchi V, Roumenina LT, 2015. Complement system part II: role in immunity. Front. Immunol 6, 257. 10.3389/fimmu.2015.00257. [PubMed: 26074922]

Meyer U, Feldon J, Dammann O, 2011. Schizophrenia and autism: both shared and disorder-specific pathogenesis via perinatal inflammation? Pediatr. Res 69 (5 Pt 2), 26R–33R. 10.1203/pdr.0b013e318212c196.

Moriyama M, Fukuhara T, Britschgi M, He Y, Narasimhan R, Villeda S, WyssCoray T, 2011. Complement receptor 2 is expressed in neural progenitor cells and regulates adult hippocampal neurogenesis. J. Neurosci 31 (11), 3981–3989. 10.1523/jneurosci.3617-10.2011. [PubMed: 21411641]

Murphy CE, Walker AK, Weickert CS, 2021. Neuroinflammation in schizophrenia: the role of nuclear factor kappa B. Transl. Psychiatry 11 (1), 528. 10.1038/s41398-021-01607-0. [PubMed: 34650030]

North HF, Weissleder C, Fullerton JM, Sager R, Webster MJ, Weickert CS, 2021. A schizophrenia subgroup with elevated inflammation displays reduced microglia, increased peripheral immune cell and altered neurogenesis marker gene expression in the subependymal zone. Transl. Psychiatry 11 (1), 635. 10.1038/s41398-021-01742-8. [PubMed: 34911938]

Patterson PH, 2009. Immune involvement in schizophrenia and autism: etiology, pathology and animal models. Behav. Brain Res 204 (2), 313–321. 10.1016/j.bbr.2008.12.016. [PubMed: 19136031]

Presumey J, Bialas AR, Carroll MC, 2017. Complement system in neural synapse elimination in development and disease. Adv. Immunol 135, 53–79. 10.1016/bs.ai.2017.06.004. [PubMed: 28826529]

Ricklin D, Hajishengallis G, Yang K, Lambris JD, 2010. Complement: a key system for immune surveillance and homeostasis. Nat. Immunol 11 (9), 785–797. 10.1038/ni.1923. [PubMed: 20720586]

Satterstrom FK, Kosmicki JA, Wang J, Breen MS, De Rubeis S, An JY, Buxbaum JD, 2020. Large-scale exome sequencing study implicates both developmental and functional changes in the neurobiology of autism. Cell 180 (3), 568–584 e523. 10.1016/j.cell.2019.12.036. [PubMed: 31981491]

Sekar A, Bialas AR, de Rivera H, Davis A, Hammond TR, Kamitaki N, McCarroll SA, 2016. Schizophrenia risk from complex variation of complement component 4. Nature 530 (7589), 177–183. 10.1038/nature16549. [PubMed: 26814963]

Sellgren CM, Sheridan SD, Gracias J, Xuan D, Fu T, Perlis RH, 2017. Patient-specific models of microglia-mediated engulfment of synapses and neural progenitors. Mol. Psychiatry 22 (2), 170–177. 10.1038/mp.2016.220. [PubMed: 27956744]

Song C, Clark SM, Vaughn CN, Nicholson JD, Murphy KJ, Mou TM, Tonelli LH, 2018. Quantitative analysis of kynurenine aminotransferase II in the adult rat brain reveals high

expression in proliferative zones and corpus callosum. Neuroscience 369, 1–14. 10.1016/j.neuroscience.2017.11.001. [PubMed: 29126954]

Spann MN, Timonen-Soivio L, Suominen A, Cheslack-Postava K, McKeague IW, Sourander A, Brown AS, 2019. Proband and familial autoimmune diseases are associated with proband diagnosis of autism spectrum disorders. J. Am. Acad. Child Adolesc. Psychiatry 58 (5), 496–505. 10.1016/j.jaac.2018.09.444. [PubMed: 30975444]

Steiner J, Walter M, Glanz W, Sarnyai Z, Bernstein HG, Vielhaber S, Stoecker W, 2013. Increased prevalence of diverse N-methyl-D-aspartate glutamate receptor antibodies in patients with an initial diagnosis of schizophrenia: specific relevance of IgG NR1a antibodies for distinction from N-methyl-D-aspartate glutamate receptor encephalitis. JAMA Psychiatry 70 (3), 271–278. 10.1001/2013.jamapsychiatry.86. [PubMed: 23344076]

Tonelli LH, Maeda S, Rapp KL, Sternberg EM, 2003. Differential induction of interleukin-I beta mRNA in the brain parenchyma of Lewis and Fischer rats after peripheral injection of lipopolysaccharides. J. Neuroimmunol 140 (1–2), 126–136. 10.1016/s0165-5728(03)00171-1. [PubMed: 12864980]

Tonelli LH, Gunsolly CA, Belyavskaya E, Atwood AR, Sternberg EM, 2004. Increased pro-thyrotropin-releasing hormone transcription in hypophysiotropic neurons of Lewis rats. J. Neuroimmunol 153 (1–2), 143–149. 10.1016/j.jneuroim.2004.05.002. [PubMed: 15265672]

Trepanier MO, Hopperton KE, Mizrahi R, Mechawar N, Bazinet RP, 2016. Postmortem evidence of cerebral inflammation in schizophrenia: a systematic review. Mol. Psychiatry 21 (8), 1009–1026. 10.1038/mp.2016.90. [PubMed: 27271499]

Vargas DL, Nascimbene C, Krishnan C, Zimmerman AW, Pardo CA, 2005. Neuroglial activation and neuroinflammation in the brain of patients with autism. Ann. Neurol 57 (1), 67–81. 10.1002/ana.20315. [PubMed: 15546155]

Velasquez E, Martins-de-Souza D, Velasquez I, Carneiro GRA, Schmitt A, Falkai P, Nogueira FCS, 2019. Quantitative subcellular proteomics of the orbitofrontal cortex of schizophrenia patients. J. Proteome Res 18 (12), 4240–4253. 10.1021/acs.jproteome.9b00398. [PubMed: 31581776]

Volk DW, Chitrapu A, Edelson JR, Roman KM, Moroco AE, Lewis DA, 2015. Molecular mechanisms and timing of cortical immune activation in schizophrenia. Am. J. Psychiatry 172 (11), 1112–1121. 10.1176/appi.ajp.2015.15010019. [PubMed: 26133963]

Volk DW, Moroco AE, Roman KM, Edelson JR, Lewis DA, 2019. The role of the nuclear factor-kappaB transcriptional complex in cortical immune activation in schizophrenia. Biol. Psychiatry 85 (1), 25–34. 10.1016/j.biopsych.2018.06.015. [PubMed: 30082065]

Walker DG, Kim SU, McGeer PL, 1998. Expression of complement C4 and C9 genes by human astrocytes. Brain Res. 809 (1), 31–38. 10.1016/s0006-8993(98)00811-7. [PubMed: 9795119]

Walport MJ, 2002. Complement and systemic lupus erythematosus. Arthritis Res. 4 (Suppl. 3), S279–S293. 10.1186/ar586. [PubMed: 12110148]

Wang C, Liu F, Liu YY, Zhao CH, You Y, Wang L, Yang Z, 2011. Identification and characterization of neuroblasts in the subventricular zone and rostral migratory stream of the adult human brain. Cell Res. 21 (11), 1534–1550. 10.1038/cr.2011.83. [PubMed: 21577236]

Wang H, Ricklin D, Lambris JD, 2017. Complement-activation fragment C4a mediates effector functions by binding as untethered agonist to protease-activated receptors 1 and 4. Proc. Natl. Acad. Sci. U. S. A 114 (41), 10948–10953. 10.1073/pnas.1707364114. [PubMed: 28973891]

Weissleder C, North HF, Bitar M, Fullerton JM, Sager R, Barry G, Shannon Weickert C, 2021. Reduced adult neurogenesis is associated with increased macrophages in the subependymal zone in schizophrenia. Mol. Psychiatry 26 (11), 6880–6895. 10.1038/s41380-021-01149-3. [PubMed: 34059796]

Yilmaz M, Yalcin E, Presumey J, Aw E, Ma M, Whelan CW, Carroll MC, 2021. Overexpression of schizophrenia susceptibility factor human complement C4A promotes excessive synaptic loss and behavioral changes in mice. Nat. Neurosci 24 (2), 214–224. 10.1038/s41593-020-00763-8. [PubMed: 33353966]

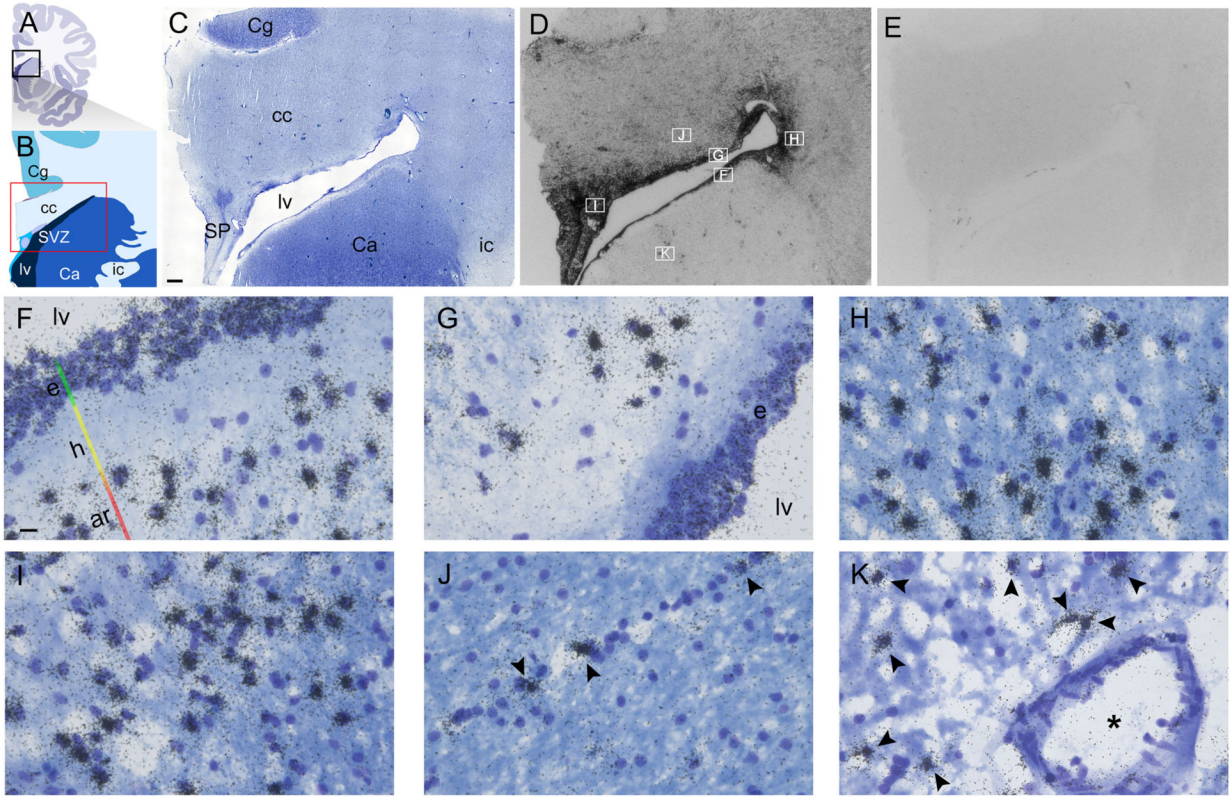

Fig. 1.

Photomicrographs of C4 *in situ* hybridization in the SVZ and surrounding areas showing the anatomical distribution of C4 mRNA. (A, B) Reference atlas showing human brain anatomy in the coronal plane: cingulate cortex (Cg), corpus callosum (cc), subventricular zone (SVZ), lateral ventricle (lv), caudate nucleus (Ca), and internal capsule (ic). Red outline indicates region used for *in situ* and RNA analyses. (C): Representative Nissl staining of a coronal section at the level of (A, B); septum pellucidum (SP). Scale bar = 1 mm. Autoradiographic images of the mRNA signal for C4 (D) and control sense probe (E). (F-K) Representative images of C4 emulsion autoradiography (400× magnification) from regions indicated in (D); scale bar = 10 μm. (F) SVZ; ependyma (e), hypocellular gap (h), astrocytic ribbon (ar); (G-H) ventricular zone; (I) SP; (J) cc and (K) *Ca*. * blood vessel.

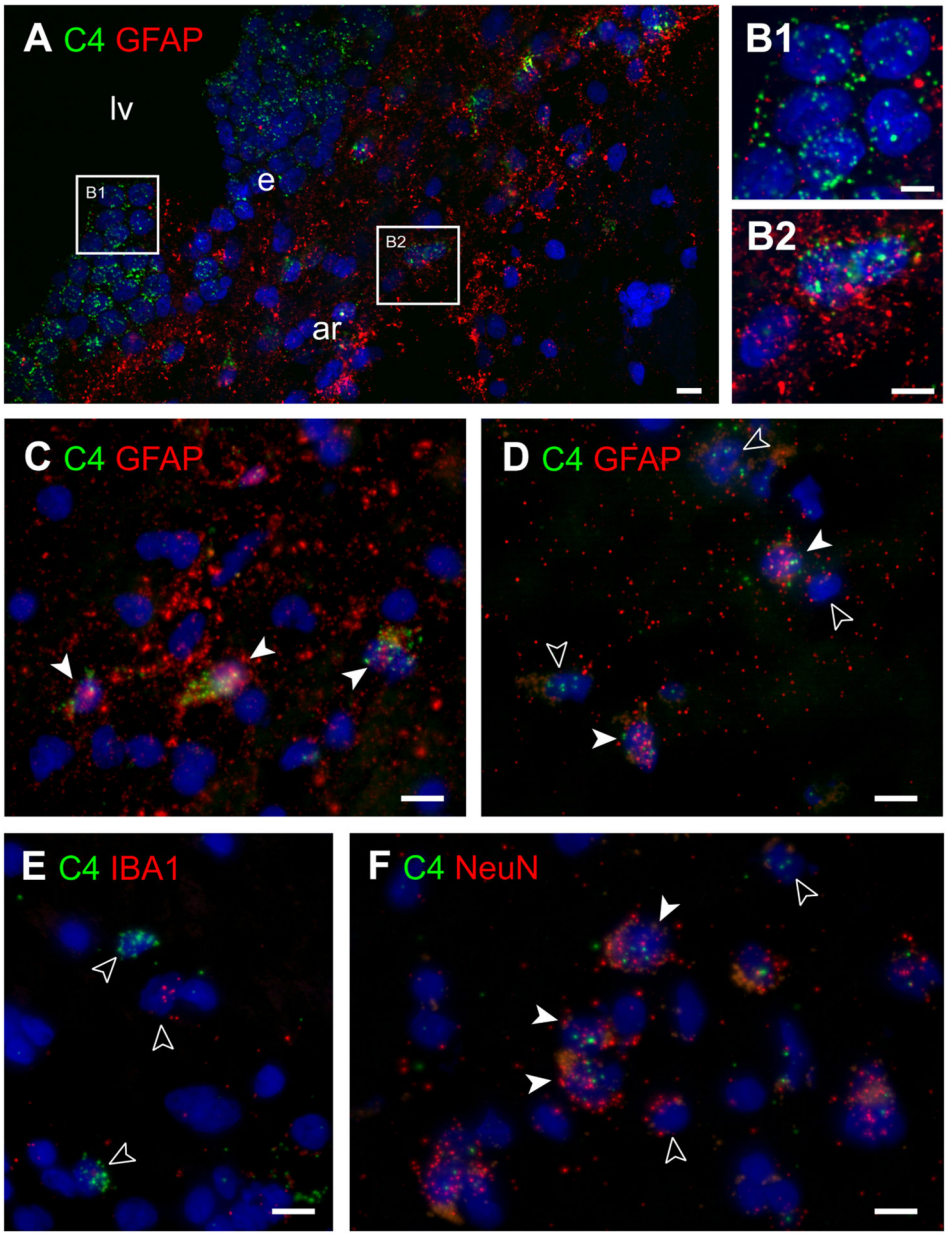

Fig. 2.

Cell-type specific expression of C4. (A) C4 (green) and GFAP (red) mRNA expression in the SVZ: lateral ventricle (lv), ependyma (e), and astrocytic ribbon (ar). (B1–2) Magnification of inserts shown in (A): ependymal cells expressing C4 (B1) and astrocytes co-expressing C4 and GFAP (B2). (C) $C4^{+}/GFAP^{+}$ astrocytes in the corpus callosum (cc), immediately dorsal to the SVZ. (D) $C4^{+}/GFAP^{+}$ astrocytes in the caudate nucleus, immediately ventral to the SVZ. (E) $Iba1^{+}$ microglia (red) do not express C4 (green) in the cc. (F) C4 (green) and NeuN (red) expression in the caudate nucleus, same area as in (D). Scale bar = 10 μm (A, C, D, E, and F); = 5 μm (B1–2). Solid arrows indicate co-expression; hollow arrows indicate single expression.

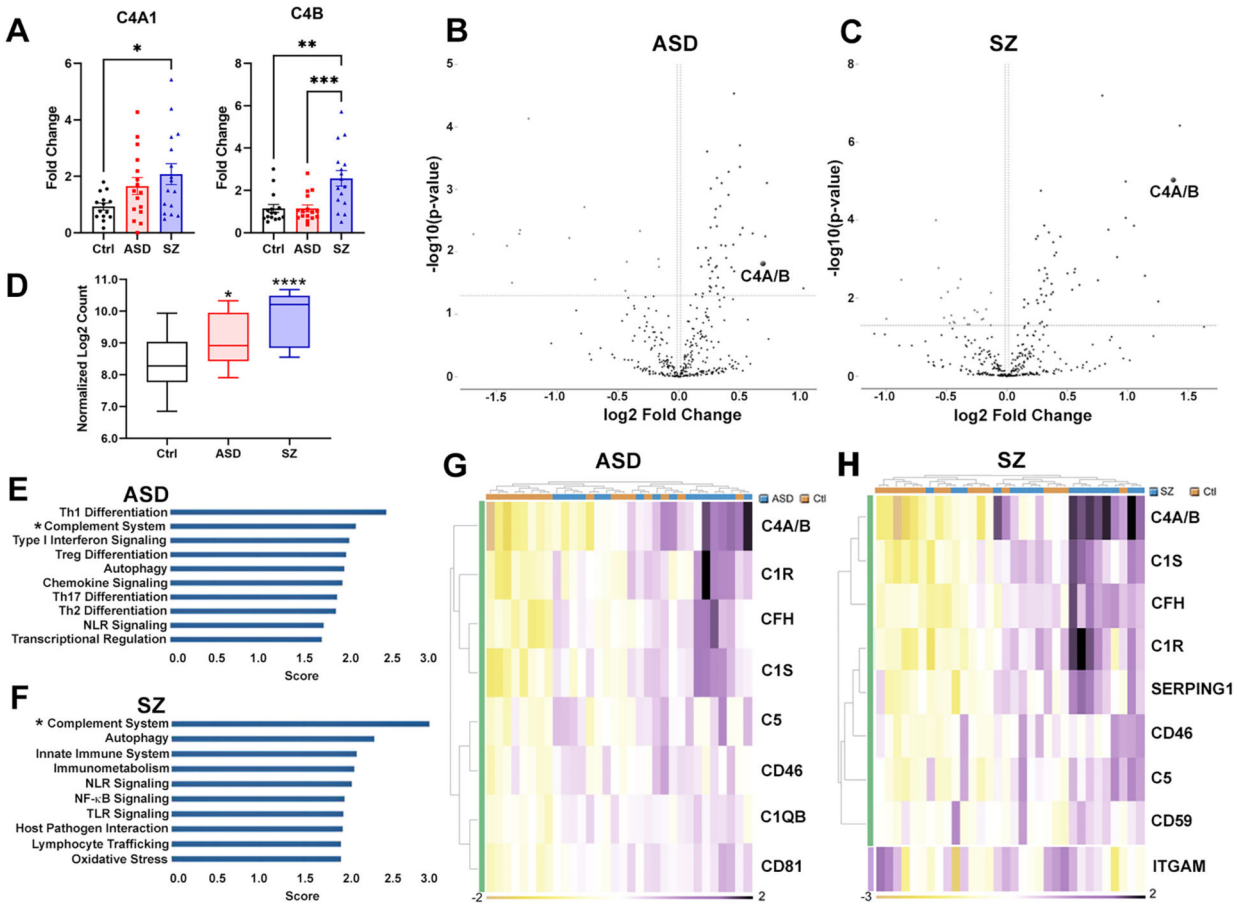

Fig. 3.

Inflammatory transcriptome analysis. (A) Quantification of mRNA expression for C4A and C4B by RT-PCR. (B, C) Volcano plots of differentially expressed genes (DEGs) ($p \geq 0.05$) in (B) autism spectrum disorder (ASD) and (C) schizophrenia (SZ) showing that C4A/B is upregulated. (D) Log2 normalized counts for C4A/B in ASD and SZ compared to controls. (E, F) Gene set analyses for (E) ASD and (F) SZ showing the top ten gene sets including DEGs. (G, H) Heatmaps of DEGs in the Complement System gene sets for (G) ASD and (H) SZ. $n = 16$/group; ANOVA with Tukey posthoc test: *$p < 0.05$; *** $p < 0.001$, **** $p < 0.0001$.

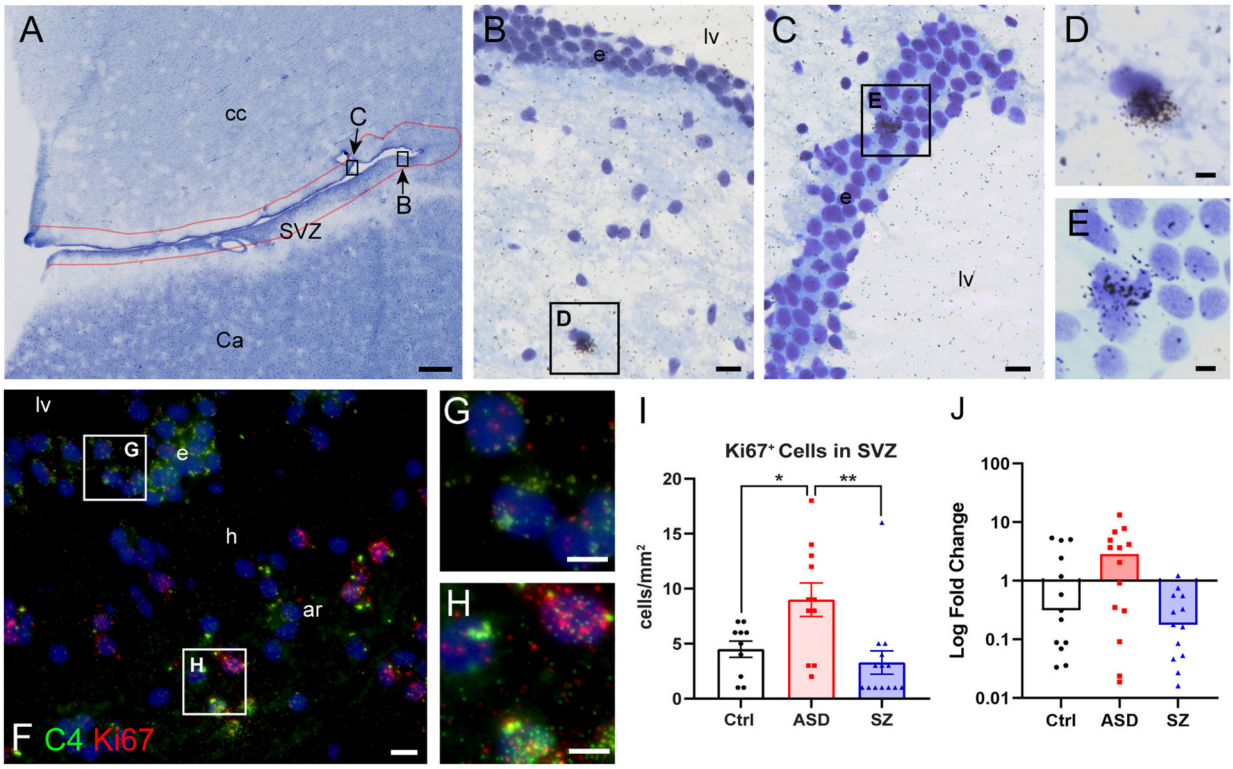

Fig. 4.

Ki67 expression in the SVZ. (A) Representative Nissl staining of a coronal section containing the SVZ. Red outline indicates the border within which Ki67$^+$ cell counting was performed. (B, C) Representative images of Ki67 emulsion autoradiography from regions indicated in (A); (B) SVZ; (C) ependyma on the dorsal border of the lateral ventricle. (D-E) Magnification of inserts shown in (B–C), showing a Ki67$^+$ cell in the SVZ (D) and Ki67$^+$ ependymal cells (E). (F) RNAscope images of C4 (green) and Ki67 (red) mRNA expression in the SVZ: lateral ventricle (lv), ependyma (e), hypocellular gap (h), astrocytic ribbon (ar). (G-H) Magnification of inserts shown in (F), confirming the co-expression of C4 and Ki67 in ependymal cells (G) and cells in the ar (H). (I) Quantification of Ki67$^+$ cells by manual counting from coronal sections shown in (A) in control (Ctrl; $n = 10$), autism spectrum disorder (ASD; $n = 11$) and schizophrenia (SZ; $n = 14$). (J) RT-PCR quantification of Ki67 mRNA ($p = 0.056$); Ctrl and SZ: $n = 13$; ASD: $n = 14$. One way ANOVA: *: $p \leq 0.05$; **: $p \leq 0.01$. Scale bar = 0.5 mm (A); 15 μm (B, C); 5 μm (D, E, G, and H); 10 μm (F).

Table 1

Demographic and tissue characteristics of post-mortem brain donors used for quantitative analyses.

Characteristics	Group (no. of tissue sample donors)		
	TD control (*n* = 16)	ASD (n = 16)	SZ (n = 16)
Age, mean ± SD, yr	21.00 ± 3.58	21.94 ± 9.28	37.81 ± 8.11
Sex, F:M	3:13	4:12	6:10
RIN, mean ± SD	7.89 ± 0.79	7.93 ± 0.81	6.72 ± 1.42
PMI, mean ± SD, h	17.63 ± 5.30	25.25 ± 9.03	19 ± 6.16
Race			
White	9	14	7
Black	7	2	9
Cause of Death			
Accidents/injuries	4	0	0
Cardiovascular	9	3	7
Neurological	0	5	1
Natural	0	1	0
Suicide	0	2	2
Substance overdose	2	0	2
Other medical conditions	1	4	3
Undetermined	0	1	1
Comorbidity			
ADHD	0	1	0
Developmental delay	0	1	0
Diabetes	0	0	1
Seizures	0	9	1

TD = typical development; ASD = autistic spectrum disorder; SZ = schizophrenia; SD = standard deviation; RIN = RNA integrity number; PMI = post-mortem interval; ADHD = attention deficit/hyperactivity disorder.